Environmental Science and Pollution Research (2020) 27:17891–17909
https://doi.org/10.1007/s11356-019-06492-1

RESEARCH ARTICLE

Promotional removal of gas-phase Hg^0 over activated coke modified by $CuCl_2$

Jie Zhang [1,2] · Caiting Li [1,2] · Xueyu Du [1,2] · Lei Gao [1,2] · Shanhong Li [1,2] · Yindi Zhang [1,2] · Zhenyu Li [1,2] · Yaoyao Yi [1,2]

Received: 6 April 2019 / Accepted: 10 September 2019 / Published online: 12 March 2020

Abstract

Impregnating $CuCl_2$ on AC (activated coke) support to synthesize $xCuCl_2$/AC showed superior activity with higher 90% Hg^0 removal efficiency at 80–140 °C, as well as a lower oxygen demand of 2% O_2 for Hg^0 removal. The acceleration on Hg^0 removal was observed for NO and SO_2. The BET, SEM, XRD, XPS, TPD, and FT-IR characterizations revealed that the larger surface area, sufficient active oxygen species and co-existence of Cu^+ and Cu^{2+} may account for the efficient Hg^0 removal. In addition, the low demand of gaseous O_2 was contributed to higher content of active oxygen and formed active Cl. After adsorbing on Cu sites, Cl sites, and surface functional groups, the $Hg^0_{(ads)}$ removal on $xCuCl_2$/AC was proceeded through two ways. Part of $Hg^0_{(ads)}$ was oxidized by active O and formed Hg^0, and the other part of Hg^0 combined with the active Cl, which was formed by the activation of lattice Cl with the aid of active O, and formed $HgCl_2$. Besides, the Hg^{2+} detected in outlet gas through mercury speciation conversion and desorption peak of $HgCl_2$ and Hg^0 further proved it. As displayed in stability test and simulated industrial application test, $CuCl_2$/AC has a promising industrial application prospect.

Keywords $CuCl_2$ · Activated coke · Elemental mercury · Adsorption · Catalytic oxidation · $HgCl_2$

Introduction

As one of the common pollutants, mercury has serious toxicity due to its high volatility, chemical stability, and bioaccumulation (Wang et al. 2010, Wu et al. 2015, Yang et al. 2016a, b). On one hand, elemental mercury and inorganic mercury chemicals could adhere to particulate matters and strengthen the toxicity of haze; on the other hand, mercury could cause serious damage on human beings and animals, such as neurotoxicity, carcinogenicity, and reproduction toxicity (Pavlish et al. 2010; Li et al. 2003). Anthropogenic mercury emission, including coal-fired plants, nonferrous metal smelting, steel production, and waste incineration, is reported to be the main cause of mercury pollution, and is threatening the human health and environmental quality (Wu et al. 2016). Among them, mercury released from coal-fired power plant has aroused attention of domestic and overseas relevant departments. The US Environmental Protection Agency (EPA) issued the national standards on the control of mercury emission, as well as some other air pollutants from coal- and oil-fired power plants (Wu et al. 2015). Ministry of Environmental Protection in China also issued the standard of mercury emission as 30 μg/m^3 for power plant. Besides, to meet the demand for the fast-developing global economy, the use of coal for power plants is still increasing sharply (Streets et al. 2011; Wu et al. 2016). Therefore, it is urgent to develop competent and cost-effective technologies on removing mercury to meet increasingly strict standard of relevant laws and regulations.

In coal-fired flue gas, the key of mercury removal is how to convert Hg^0, with high volatility, stability, and low water solubility, into Hg^P or Hg^{2+}, while Hg^P and Hg^{2+} could be captured by the existing dust-cleaning apparatus and wet flue gas desulfurization (WFGD) system, respectively (He et al. 2009). Among numerous technologies, such as adsorption (Yang et al. 2007), catalytic oxidation (Zhang et al. 2017a), activated carbon injection (ACI) (Wu et al. 2017), photocatalysis (Hsi and Tsai 2012), and so on, ACI

Responsible editor: Philippe Garrigues

✉ Caiting Li
ctli@hnu.edu.cn

[1] College of Environmental Science and Engineering, Hunan University, Changsha 410082, China

[2] Key Laboratory of Environmental Biology and Pollution Control, Hunan University, Ministry of Education, Changsha 410082, China

has been recognized as one of the most effective method for Hg^0 removal in practical application (Sjostrom et al. 2010). However, high operation cost of ACI, including the high production cost and inferior regeneration performance of activated carbon, has still inhibited its wide application (Granite et al. 2000; Granite et al. 2007). Therefore, various sorbents, as the alternative for activated carbon, have been investigated for Hg^0 removal, such as carbon-based sorbent (Wu et al. 2017; Qu et al. 2018), zeolite (Abrishamkar and Kahkeshi 2013), fly ash (Yang et al. 2016a, b), Ca-based sorbent (Ghorishi et al. 2011), and so on. Among them, activated coke (AC) has been proved to be efficient in the existing combined desulfuration and denitration system because of its porous structure and abundant surface groups (Sheng et al. 2017). In particular, AC not only exhibits adsorption capacity and catalytic activity similar to activated carbon, but also possesses superior mechanical strength and better regeneration performance (Tsuji and Shiraishi 1990, 1997). Besides, as one product of low-quality coal, AC owns lower production cost and can be used as good supporter in industrial fluidized bed technology due to high abrasion resistance. Even though, the performance of Hg^0 purification using virgin AC is still restricted by its limited physic-chemical properties. Especially, its smaller surface area and lower content of oxygen-contained functional groups would inhibit the physisorption and chemisorption of Hg^0, respectively (Sun et al. 2017; Zhang et al. 2015). Therefore, it is important to explore valid modification methods of AC support to realize the enhancement of its specific surface area and surface oxygen-contained functional groups, thus improving its adsorption and redox capacity for effective Hg^0 removal.

For purpose of improving the activity of AC, modification with metal oxides, such as MnO_x (He et al. 2014; Zhou et al. 2016a, b), CeO_2 (He et al. 2016; Zhang et al. 2016), Fe_2O_3 (Wang et al. 2016), Co_3O_4 (Zhang et al. 2014), CuO (Zhao et al. 2016b), and even bimetal oxides (Li et al. 2012; Kan et al. 2017; Wu et al. 2017), was found to be an effective approach to optimize the property of support. Besides, halogen has also been proved to be an alternative for improving the activity of Hg^0 removal (Zeng et al. 2017; Tang et al. 2018). Thereinto, chlorine is an effective oxidant for Hg^0 oxidation with the aid of O_2 and could be derived from HCl through the Deacon reaction (Presto and Granite 2006), Eley-Rideal mechanism (Niksa and Fujiwara 2005), or Langmuir-Hinshelwood (Senior 2012). Nevertheless, the chlorine contained in coal-fired flue gas could not always respond to the request of Hg^0 removal. In previous studies, supported $CuCl_2$ sorbents or catalysts were proved to present good performance for Hg^0 removal (Kim et al. 2010; Li et al. 2013a, b; Liu et al. 2015). Liu et al. (Liu et al. 2015) reported there existed both Cu sites and Cl sites for the adsorption of Hg^0, and then the adsorbed Hg^0 was oxidized by amorphous $CuCl_2$ via losing Cl. Besides, the formed CuCl could be regenerated into $CuCl_2$ with the co-existence of hydrogen chloride and O_2. Zhou et al. (2016b) found that the chemical adsorbed oxygen would activate HCl to form active chlorine species at low temperature, thus exhibiting a superior Hg^0 removal activity. And in their study afterwards (Zhou et al. 2018), they found that the active chlorine species, as the direct oxidant for Hg^0, could also be formed through the interaction between the lattice Cl in amorphous $CuCl_2$ and chemical adsorbed oxygen species. However, as far as known, the $CuCl_2$ possesses the weak chemical adsorbed oxygen storage, which is not sufficient for the activation of lattice Cl. With various surface functional groups and active adsorption sites, AC could be selected as support to provide chemical adsorbed oxygen to some extent. Therefore, the assumption for the $CuCl_2$-modified AC to improve Hg^0 removal activity under the atmosphere without HCl was encouraged. Unfortunately, few study on using $CuCl_2$/AC for the Hg^0 removal both in bench scale and in simulated industrial application test was reported. In addition, the specific mechanism on Hg^0 removal over $CuCl_2$/AC was still not clear.

In this study, $CuCl_2$/AC prepared by impregnation method with different $CuCl_2$ loading was tested for Hg^0 removal. The N_2 adsorption-desorption isotherm, SEM, XRD, XPS, Hg-TPD, and FT-IR were carried out to investigate the physic-chemical properties and discuss the role of $CuCl_2$ and AC on Hg^0 removal, as well as the effect of SO_2 and NO on Hg^0 removal. On the basis of the above study, the mechanism of Hg^0 removal was proposed. Moreover, to investigate its potential in industrial application, simulated industrial application test was also conducted for Hg^0 removal using virgin and regenerated columnar AC modified with $CuCl_2$.

Experimental

Sample preparation

In this study, the AC was provided by Ke'xing Carbon Industry, Inner Mongolia. The columnar AC was firstly smashed, sieved, and washed with deionized water to obtain the required AC powder with the diameter of 0.125–0.180 mm. To remove the residual impurity in the pore, the powder was placed under ultrasonic oscillation for 30 min and then rinsed five times again. Finally, the sample was dried at 105 °C for 24 h.

The $CuCl_2$/AC was prepared by impregnation method in this study. Firstly, 0.25 g, 0.48 g, and 1.01 g $CuCl_2{\cdot}2H_2O$ was dissolved homogeneously in 50 mL absolute ethyl alcohol, respectively. And each 5 g AC sample was placed into three obtained solutions, respectively, and kept under magnetic stirring for 8 h. Then the mixtures were filtered with qualitative filter paper (Xinxing, $D = 11$ cm) with the filtering velocity of

35–70 s followed by washing with 20 mL absolute ethyl alcohol repeatedly. The obtained final samples were placed in drying oven and maintained at 105 °C for 12 h to acquire modified activated coke with different $CuCl_2$ loading. Besides, the atom adsorption spectrometry was performed to detect the content of copper contained in the residual filtrate. And the actual content of loaded $CuCl_2$ was calculated as the difference between dissolved $CuCl_2$ and the residual $CuCl_2$ in filtrate. The samples were denoted as xCuCl$_2$/AC, where x was the mass ratio of $CuCl_2$/AC (x = 2.2%, 4.5% and 5.7%, respectively).

In simulated industrial application test, both fresh cylinder activated coke (CAC) and CAC after cyclic regeneration for 1–3 and more than 8 times, which was roughly estimated by the abrasion of AC, were obtained from the combined desulfurization and denitration unit (Wengfu, Guizhou, China) using AC provided from Ke'xing Carbon Industry in China, which were denoted as CAC, CAC-3, and CAC-8, respectively. 1.01 g $CuCl_2$ was dissolved in homogeneously in 50 mL absolute ethyl alcohol used as the manual sprayer. The sample was set in shaking bed and maintained rolling and moving, and then was sprayed with $CuCl_2$ solution (50 g CAC/8 mL spray solution). After drying the sample at 105 °C for 6 h, the resulted $CuCl_2$/CAC, $CuCl_2$/CAC-3 and $CuCl_2$/CAC-8 was obtained.

Mercury removal experiment

Mercury removal performance test was carried out in a bench-scale removal system, similar to our previous work (Fan et al. 2012). The different samples were placed in a temperature-controlled fixed-bed reactor (10-mm internal diameter) to maintain at the desired reaction temperature. The simulated flue gas including 6% O_2 and 70 μg/m^3 Hg^0 balanced by N_2 passed through the fixed-bed reactor with the flow rate of 500 mL/min. The Hg^0 concentration was monitored by an online mercury analyzer (Lumex RA-915M, Russia) in the inlet and outlet flue gas. As shown in Table 1, 0.1 g sample was used in the performance tests, while only 0.05 g sample was applied, for the purpose of enlarging the difference, when investigating the effect of gas components (O_2, HCl, SO_2, and NO) as well as the mercury conversion experiment, corresponding to the gas hourly speed velocity (GHSV) of 200000 h^{-1} and 400000 h^{-1}, respectively. Note that, in simulated industrial application test, 50 g columnar AC was placed under the atmosphere which contained 70 μg/m^3 Hg^0 + 6% O_2/N_2 with a gas flow rate of 500 mL/min, that is with the GHSV of 500 h^{-1} similar to the actual GHSV in industrial application. Besides, due to the research focusing on ACI technology, the initial performance during 60 min was conducted at the temperature range of 80–200 °C. To better investigate the Hg^0 adsorption and Hg^0 oxidation on xCuCl$_2$/AC, the mercury speciation conversion system consisting of two paths was employed between the fix-bed reactor and mercury online analyzer (Tao et al. 2012). One path was placed with 10% KCl solution to capture the oxidized mercury (Hg^{2+}), so that only Hg^0 in simulated flue gas (Hg^0_{out}) was detected. For the other path, Hg^{2+} was transformed into Hg^0 through 0.5 mol/L $SnCl_2$/HCl solution, and the measured concentration was denoted as HgT out. And all the experiments were performed repeatedly for three times to ensure the accuracy and reliability of the obtained data.

The total Hg^0 removal efficiency (E_T), the Hg^0 adsorption efficiency (E_{ads}), and the Hg^0 oxidation efficiency (E_{oxi}) were calculated as the following equation:

$$E_T = \frac{Hg^0_{in} - Hg^0_{out}}{Hg^0_{in}} \times 100\% \quad (1)$$

$$E_{ads} = \frac{Hg^0_{in} - Hg^T_{out}}{Hg^0_{in}} \times 100\% \quad (2)$$

$$E_{oxi} = \frac{Hg^T_{out} - Hg^0_{out}}{Hg^0_{in}} \times 100\% \quad (3)$$

$$E_T = E_{ads} + E_{oxi} \quad (4)$$

To identify the mercury species formed on the treated samples, Hg-TPD was conducted for 4.5% $CuCl_2$/AC treated in different atmospheres. 0.35 g sample was firstly exposed to 100 g/cm^3 Hg^0 + 400 ppm SO_2/500 ppm NO (when used) + 6% O_2/N_2 with a flow rate of 500 mL/min and treated at 140 °C for 6 h. After cooled down to room temperature, the sample was heated to 600 °C under N_2 atmosphere with the heating rate of 5 °C/min. And the concentration of Hg^0 desorbed from sample was detected online by RA-915M mercury analyzer (LUMEX Ltd, Russia).

Sample characterization

To investigate the physic-chemical properties of samples, the following characterizations were conducted.

The actual content of metal doping over AC was measured by inductively coupled plasma-atomic emission spectrometry (ICP-AES, SPECTRO BLUE SOP, Germany).

The scanning electron microscopy (SEM) graphs were taken on a JSM-6700F (Japan) instrument to study the morphology and microstructure of samples.

The textural properties of x$CuCl_2$/AC and virgin AC containing BET surface area, pore volume, and average pore diameter were carried out on a Micromeritics Tristar II 3020 analyzer (Micromeritics Instrument Crop, USA).

Powder X-ray diffraction (XRD) patterns determining the crystal form of different samples were carried out on a Rigaku rotaflex D/Max2500 powder diffractometer (Rigaku, Japan) with Cu-Ka radiation (40 kV, 250 mA) in a scanning range of 10–80° (2θ).

To obtain the chemical states of active constituent element, X-ray photoelectron spectroscopy (XPS) analysis was

Table 1 The experimental reaction conditions

	Sample	Flue gas (500 mL/min)	Temperature (°C)
Set I	xCuCl$_2$/AC (x = 0–5.7%) (0.1 g)	70 μg/m^3 Hg^0, 6% O_2, N_2	80–200
Set II	4.5% CuCl$_2$/AC (0.05 g)	70 μg/m^3 Hg^0, 0–6% O_2, 0–800 ppm SO_2, 0–1000 ppm NO, 0–20 ppm HCl, N_2	The optimal temperature
Set III	xCuCl$_2$/AC (x = 2.2–5.7%) (0.05 g)	70 μg/m^3 Hg^0, 0–6% O_2 , N_2	The optimal temperature
Set IV	4.5% CuCl$_2$/AC (0.1 g)	70 μg/m^3 Hg^0 , 6% O_2, N_2	110, 140
Set V	CAC, CuCl$_2$/CAC, CuCl$_2$/CAC-3, CuCl$_2$/CAC-8 (50 g)	70 μg/m^3 Hg^0, 0–6% O_2, 400 ppm SO_2, 500 ppm NO, N_2	The optimal temperature

measured on a K-Alpha 1063 spectrometer (Thermo Fisher Scientific, USA).

Fourier-transform infrared spectroscopy (FT-IR, Shimadzu, Japan) was carried out to qualitatively analyze the surface functional groups of obtained samples. And the used samples were treated under the 500 mL/min flow of 6% O_2 + 70 μg/m^3 Hg^0 + N_2 at 140 °C for 4 h. Prior to each measurement, the sample was purged by 500 mL/min N_2 at 120 °C to eliminate the effect of impurity and moisture.

Results and discussion

The performance of samples

To investigate the role of $CuCl_2$, the AC modified with different loading values of $CuCl_2$, including virgin AC, low concentration (2.2%), moderate concentration (4.5%), and high concentration (5.7%), were examined for Hg^0 removal.

The Hg^0 removal on virgin AC is illustrated in Fig. 1. For all examined reaction temperature, the Hg^0 removal efficiency of virgin AC decreased sharply to nearly zero within 30 min, except for the reaction at 140 °C. In terms of Hg^0 removal at 140 °C, the virgin AC exhibited the initial Hg^0 removal efficiency (E_T) of 21.80%, and the decrease tendency started to slow down after reacted for 10 min, which lasted for 30 min. The Hg^0 removal over virgin AC might be mainly contributed to its pore structure and the surface functional groups, where the pore structure mostly participated in the physisorption and surface functional groups contributed to the chemisorption (Sun et al. 2017; Zhang et al. 2015). However, it was not sufficient for long-time Hg^0 removal. Therefore, virgin AC was modified with different content of $CuCl_2$ and was conducted for performance test as follows.

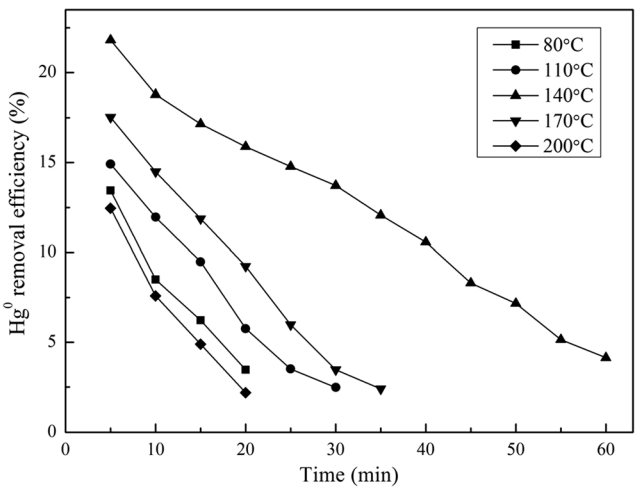

Fig. 1 Removal efficiency of Hg^0 on virgin AC in simulated flue gas (reaction condition 0.1 g sample, 6% O_2, 70 μg/m^3 Hg^0, N_2 as balance gas, T = 80–200 °C, total flow rate 500 mL/min)

As depicted in Fig. 2, all three modified AC with different $CuCl_2$ content exhibited the similar trend for Hg^0 removal at 80–200 °C. For all $x CuCl_2$/AC samples, E_T firstly enhanced with the increasing temperature, and reached as high as near 100% at 110 and 140 °C. And regardless of the loading value of $CuCl_2$, no obvious change was observed for Hg^0 removal efficiency at lower temperature, especially on 4.5% $CuCl_2$ and 5.7% $CuCl_2$/AC. However, the further increase of temperature resulted in the declined tendency of Hg^0 removal. Besides, there existed a positive correlation between the $CuCl_2$ loading and Hg^0 removal activity at 170–200 °C. When reaction proceeded for 60 min, almost 75% and 45% Hg^0 removal efficiency were reached for 2.2% $CuCl_2$/AC at 170 and 200 °C (Fig. 2a), and an increase of 5% and 15% occurred on 5.7% $CuCl_2$/AC, respectively (Fig. 2c). In other words, the addition of $CuCl_2$ promoted the Hg^0 removal performance of AC markedly, and broadened the reaction temperature window, which was conductive to its practical application. And in consideration of economy in practical application, 4.5% $CuCl_2$/AC was chosen as optimal sample in the following study.

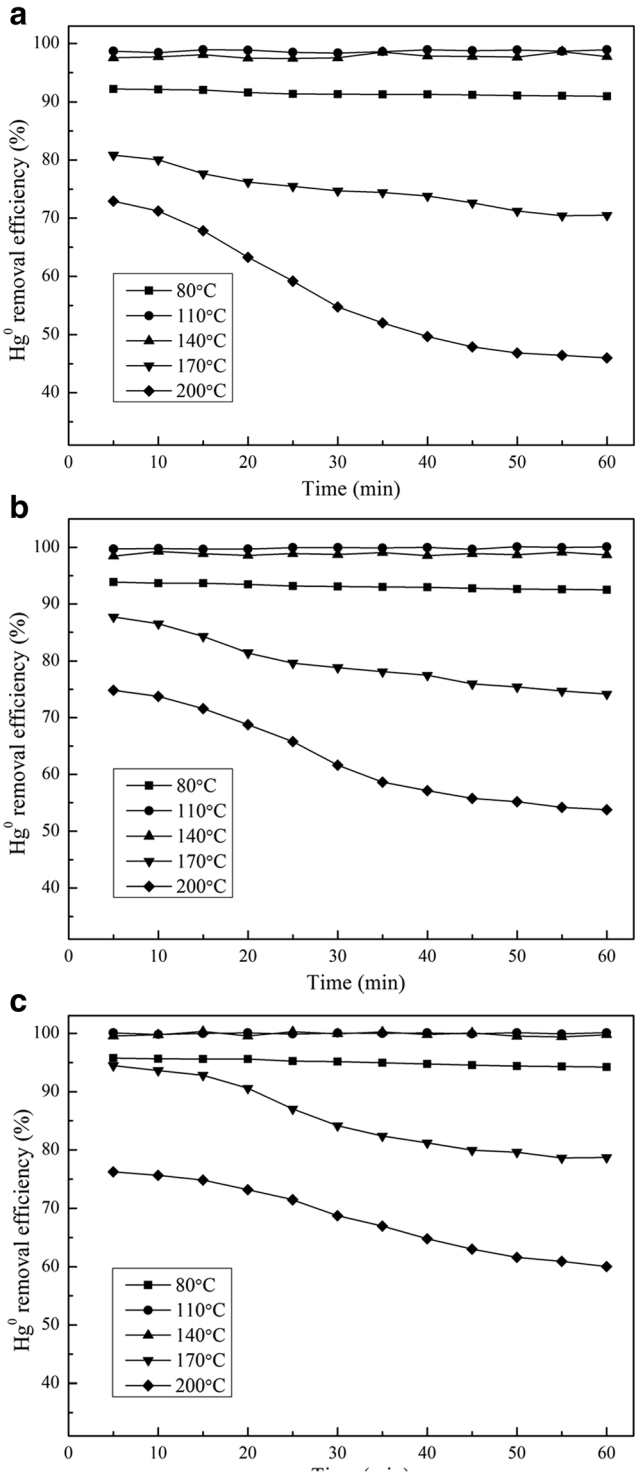

Fig. 2 Removal efficiency of Hg^0 on **a** 2.2% $CuCl_2$/AC, **b** 4.5% $CuCl_2$/AC, and **c** 5.7% $CuCl_2$/AC in simulated flue gas (reaction condition 0.1 g sample, 6% O_2, 70 μg/m^3 Hg^0, N_2 as balance gas, T = 80–200 °C, total flow rate 500 mL/min)

Effect of gas components

Effect of O_2 and HCl

The influence of gas components on the Hg^0 removal efficiency of 4.5% $CuCl_2$/AC is depicted in Fig. 3. Only 72.38% of Hg^0 removal efficiency was reached under pure N_2. Obviously, the addition of O_2 significantly enhanced the Hg^0 removal activity of samples, especially a significant increase with 1–2% O_2, and the further increase of oxygen concentration to 6–12% only led to a negligible increase of Hg removal efficiency. The sharp increase might be caused by the replenishment of surface active oxygen (O^*) consumed in Hg^0 removal by gas-phase O_2. On one hand, O^* bonded with Hg^0

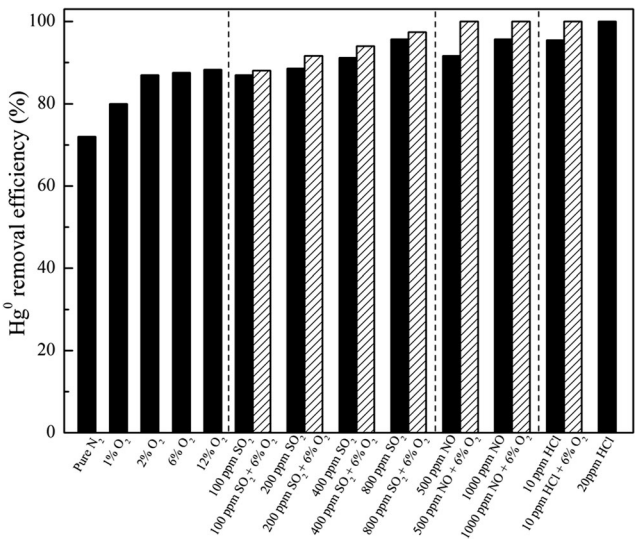

Fig. 3 The effect of individual flue gas components on the removal of Hg^0 over 4.5% $CuCl_2$/AC (reaction condition 0.05 g sample, 0–6% O_2, 0–800 ppm SO_2, 0–1000 ppm NO, 0–20 ppm HCl, 70 μg/m^3 Hg^0, N_2 as balance gas, T = 140 °C, total flow rate 500 mL/min, reaction time 60 min)

adsorbed on the surface and formed Hg^0 (Tang et al. 2018). On the other hand, O^* could activate the lattice Cl in amorphous $CuCl_2$, and the resulted active Cl could also oxidize Hg^0 (Yang et al. 2016b). In this study, 2% O_2 could meet the demand of Hg^0 removal on 4.5% $CuCl_2$/AC, which was lower than 3% or 6% in other previous studies (Wu et al. 2015; Zeng et al. 2017; Tang et al. 2018). Undoubtedly, abundant active surface oxygen generated during the $CuCl_2$/AC modification process, and active Cl originated from $CuCl_2$ also contributed to the additional Hg^0 removal approach (Li et al. 2013a, b), which will be discussed in the following characterizations.

As the major halogen species in coals, chlorine appears mainly as HCl after combustion in coal-fired flue gas (Zhuang et al. 2007). In this study, a significant promotion effect of HCl was observed for 4.5% $CuCl_2$/AC. When adding 10 ppm HCl into pure N_2, 95.42% Hg^0 removal efficiency was reached, which was much higher than that observed under pure N_2. Besides, the promotion effect was further strengthened by the increased HCl concentration and the addition of O_2, and nearly 100% Hg^0 removal efficiency was observed. Two aspects might be responsible for the positive effect of HCl on Hg^0 removal. On one hand, with the aid of active oxygen, HCl could be transformed into active chlorine species, which contributed to both adsorption and oxidation of Hg^0 (Zhuang et al. 2007; Cao et al. 2007). On the other hand, Cu_2OCl_2 was reported as one of the intermediates during Hg^0 removal, and it could be converted into $CuCl_2$ with the presence of HCl (Yang et al. 2016b).

Effect of SO_2 and NO

As one of the typical components in coal-fired flue gas, SO_2 has a crucial role in Hg^0 removal because of the complex interaction between SO_2 and Hg^0 on sample surface (Zhuang et al. 2007; Li et al. 2013c). However, the specific effect of SO_2 on Hg^0 removal was still indefinite. Li et al. (2011a, b) found that 1200 ppm SO_2 exhibited a promotion role due to the generation of active species that was in favor of Hg^0 oxidation. In some other studies, SO_2 was reported to adversely affect the Hg^0 removal through the competitive adsorption between SO_2/SO_3 and Hg^0, as well as the consumption of surface Cl on account of the formation of sulfuryl chloride (Kim et al. 2010; Li et al. 2013c). However, in this study, with the absence of O_2, SO_2 exhibited the promotion effect on Hg^0 removal, and the acceleration became more obvious with increasing SO_2 concentration, as depicted in Fig. 3. And the supply of O_2 further facilitated the Hg^0 removal on 4.5% $CuCl_2$/AC. It was speculated that the promotion effect might result from the formation of SO_3, which was contributed to S-bonded chemisorption, through the oxidation of SO_2 by abundant active oxygen, as well as the redox cycle Cu^{2+}/Cu^+, and then formed $HgSO_4$ and $HgSO_3$ (Jeong et al. 1999; Li et al. 2011a, b; Tan et al. 2012). In addition, Cu was reported to possess larger affinity to sulfur, thus protecting active Cl from the deactivation of SO_2 (Wang et al. 2013). The aid of O_2 could not only replenish the active oxygen occupied by SO_2, but also provide more active oxygen for the formation of SO_3, thus further promoting the Hg^0 removal. From the above, with a high capacity of SO_2 resistance, $CuCl_2$-modified AC possessed huge potential for application in coal-fired power plants with high content of SO_2 or without desulfurization pretreatment.

When adding 500 and 1000 ppm NO into pure N_2, an increase of 19.85% and 23.24% for Hg^0 removal efficiency was achieved on 4.5% $CuCl_2$/AC, respectively. With abundant active oxygen, NO would be converted into NO_2 on the surface of 4.5% $CuCl_2$/AC (Aissat et al. 2011). As a stronger oxidant than O_2, NO_2 could directly react with Hg^0 and formed $Hg(NO_3)_2$ (Norton et al. 2003; Jin et al. 2010; Fuente-Cuesta et al. 2012). Moreover, at the presence of O_2, 100% removal efficiency was achieved under both two atmospheres (500/1000 ppm NO + 6% O_2). On one hand, the addition of O_2 could supplement more surface active oxygen for the oxidation of NO. On the other hand, the generation of $Hg(NO_3)_2$ was facilitated by O_2 through the reaction $Hg^0 + O_2 + NO/NO_2 \rightarrow Hg(NO_3)_2$. And the specific mechanism will be investigated in detail afterwards.

Mercury speciation conversion test

The Hg^0 adsorption efficiency (E_{ads}) and Hg^0 oxidation efficiency (E_{oxi}) over $x$$CuCl_2$/AC were distinguished by mercury speciation conversion experiment, as shown in Fig. 4. Both E_T and E_{oxi} increased with the increasing loading value of $CuCl_2$ in pure N_2, indicating higher $CuCl_2$ content might result in more active surface

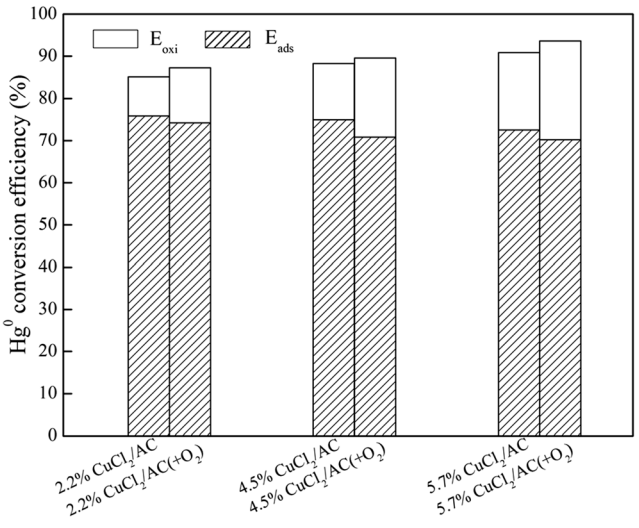

Fig. 4 Hg^0 adsorption efficiency and Hg^0 oxidation efficiency over $x$$CuCl_2$/AC (reaction condition 0.05 g sample, 0–6% O_2, 70 μg/m^3 Hg^0, N_2 as balance gas, T = 140 °C, total flow rate 500 mL/min, reaction time 60 min)

oxygen, active chlorine, and Cu sites for both adsorption and oxidation of Hg^0. Similar phenomenon was also found by Yang et al. (2016a). Notably, the addition of 6% O_2 contributed to a distinct increase of 3.78%, 5.37%, and 5.04% for Hg^0 oxidation efficiency on 2.2% $CuCl_2$/AC, 4.5% $CuCl_2$/AC, and 5.7% $CuCl_2$/AC, respectively, while a slight decrease for Hg^0 adsorption efficiency. The competitive adsorption between gas-phase O_2 and elemental mercury, as well as the further oxidation of adsorbed Hg^0 and the following desorption of formed Hg^0, should be responsible for the decrease of E_{ads}, as reported by the previous study (Zeng et al. 2017). It could be deduced that adsorption still was the main removal mechanism for Hg^0 on $x$$CuCl_2$/AC, and oxidation was promoted with increasing $CuCl_2$ content, as well as the presence of O_2, which would be testified in the following characterizations.

Stability test

The stability of 4.5% $CuCl_2$/AC for Hg^0 removal was measured at 110 and 140 °C for 2160 min, respectively. As depicted in Fig. 5, no obvious deactivation occurred, and Hg^0 removal efficiency maintained over 99.50% at 140 °C until the reaction proceeded 960 min. And then the Hg^0 removal efficiency decreased to 92.26% after treated with Hg^0 for 2160 min. Although the similar initial Hg^0 removal efficiency was exhibited, an obvious decrease of 23%, with the gradually sharper decrease tendency, was observed for 4.5% $CuCl_2$/AC after reacted for 2160 min at 110 °C. As seen from Fig. 4, both adsorption, as the crucial role, and oxidation contributed to Hg^0 removal over $x$$CuCl_2$/AC. And with increasing temperature, physisorption would be inhibited, while chemisorption and oxidation would be facilitated.

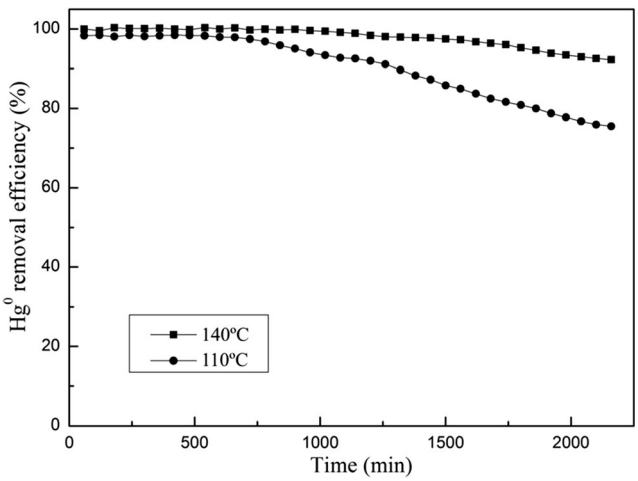

Fig. 5 Stability test of Hg^0 removal over 4.5% $CuCl_2$/AC (reaction condition 0.1 g sample, 6% O_2, 70 μg/m^3 Hg^0, N_2 as balance gas, T = 110 and 140 °C, total flow rate 500 L/min, reaction time 2160 min)

According to stability test, 4.5% $CuCl_2$/AC possessed a better stability at 140 °C than that at 110 °C, implying the chemisorption, rather than physisorption, played the predominant role in Hg^0 removal using 4.5% $CuCl_2$/AC. Zeng et al. (2017) also revealed that the dominating removal approach for Hg^0 with AC turned from physical adsorption into chemical adsorption after impregnated with halide ions. Moreover, the promotion of oxidation by increasing temperature was also responsible for the higher Hg^0 removal efficiency at 140 °C. Therefore, 4.5% $CuCl_2$ possesses great potential for low-temperature Hg^0 removal in practical industry application.

Characterization of materials

ICP-AES

The content loaded on sample with different loading values measured by ICP-AES is presented in Table 2. It was observed that there was only a small difference between the content of Cu calculated through the experiment and that measured by ICP-AES. Notably, both two actual contents measured were far less than the actual content, and the difference increased with the $CuCl_2$ dissolved in the impregnation liquid.

SEM

SEM characterization was conducted to investigate the morphology of samples, as shown in Fig. 6. Comparing virgin AC with $x$$CuCl_2$/AC, obvious difference was observed. For virgin AC (Fig. 6d), there existed blocky plane structure with layered microcrystalline texture, similar to graphite, on the surface. And the adjacent microcrystalline textures with different shapes and sizes would extrude with each other, resulting in the irregular collapse or pore structure in the interlayers.

Table 2 The content (wt%) of Cu in sample obtained by experiment and ICP-AES

Sample	Cu content (wt%)		
	Nominal content	Actual content	
		[a]Experiment	[b]ICP-AES
2.2% $CuCl_2$/AC	2.35	1.04	1.12
4.5% $CuCl_2$/AC	4.52	2.12	2.31
5.7% $CuCl_2$/AC	9.51	2.68	2.92

[a] The Cu content loaded on sample calculated by the difference between dissolved $CuCl_2$ and the residual $CuCl_2$ in filtrate as described in the manuscript

[b] The Cu content loaded on sample measured by ICP-AES

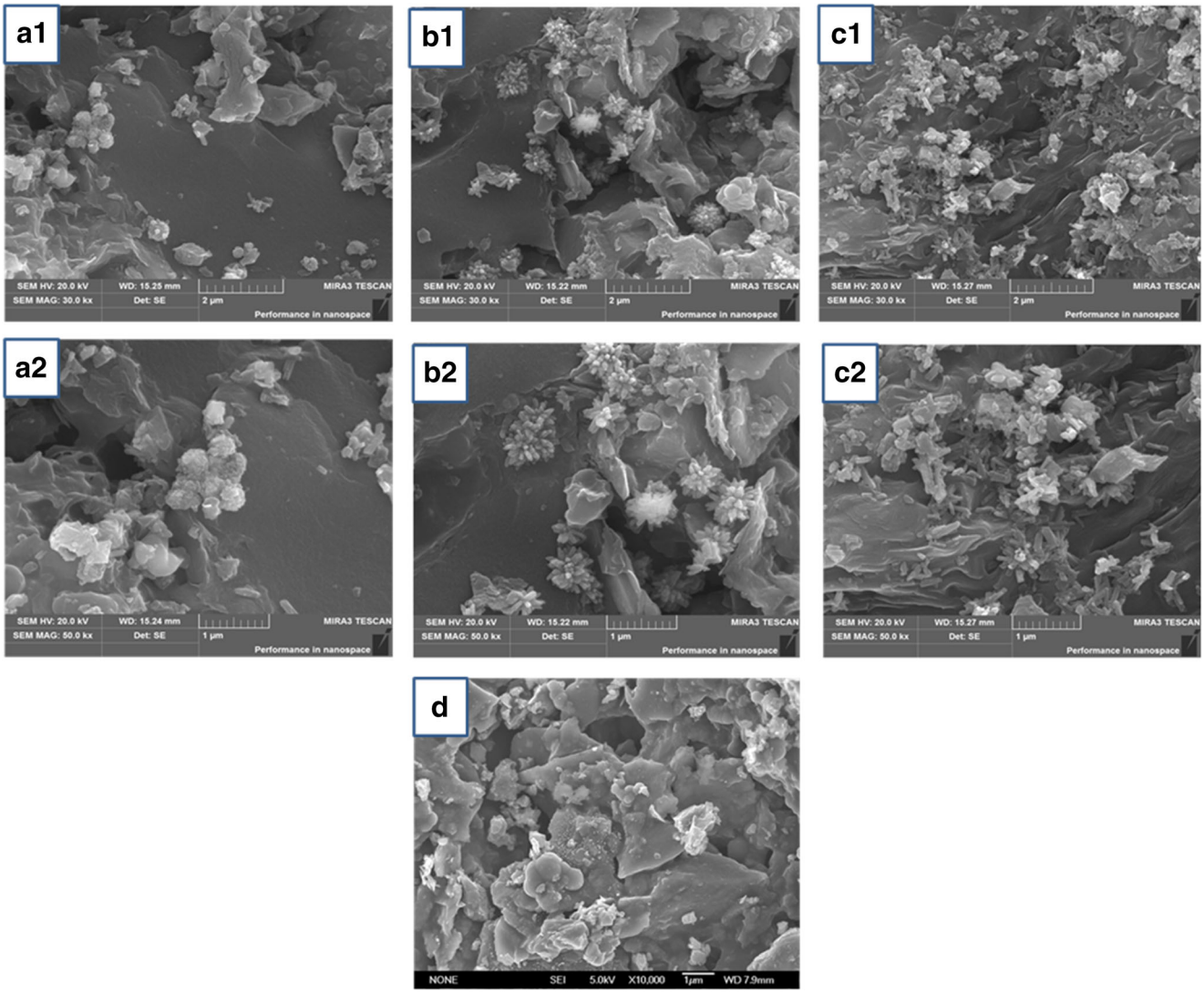

Fig. 6 SEM images (1) × 30000 and (2) × 50000 of **a** 2.2% $CuCl_2$/AC, **b** 4.5% $CuCl_2$/AC, and **c** 5.7% $CuCl_2$/AC and **d** virgin AC (× 10000).

After $CuCl_2$ doped, active components were observed on the surface of sample, as well as in the pores, with various morphological characteristics. The active components existed as spherical particles with smaller semicircular protuberances over the surface of 2.2% $CuCl_2$/AC. As loading value of $CuCl_2$ increased to 4.5%, the spherical particles evolved into the flower-like structure, and a few of them entered into the pore of AC. The flower-like structure could endow the sample with a larger surface area, thus not only promoting the mobility of gas-phase O_2 on the surface, but providing more active sites for both adsorption and oxidation of Hg^0 (Du et al. 2018a, b). After $CuCl_2$ doped, active components were observed on the surface of sample, as well as in the pores, with various morphological characteristics. Moreover, the active components over 5.7% $CuCl_2$ gradually agglomerated in the collapse and pore structure of sample, thus blocking some pores and providing fewer active sites for Hg^0 removal.

BET

As shown in Table 3, the BET surface area, pore volume, and average pore size were calculated by N_2 adsorption-desorption isotherm. In comparison with virgin AC, the surface area of $x$$CuCl_2$/AC was distinctly improved, while a slight decrease was observed for the pore volume and average pore diameter. Combining with SEM (Fig. 6), the increase on

Table 3 BET surface and pore parameters of the different samples

Samples	BET surface area (m^2/g)	Pore volume (cm^3/g)	Average pore diameter (nm)
Virgin AC	237.63	0.121	2.048
2.2% $CuCl_2$/AC	271.48	0.101	2.041
4.5% $CuCl_2$/AC	284.50	0.107	2.037
5.7% $CuCl_2$/AC	288.62	0.116	1.936

surface area might be caused by the active components dispersed on the surface of AC. However, the dispersion of the active components in the pore and the formation of collapse structure led to a decrease on pore volume and average pore diameter. Moreover, the generation of new micropores during the impregnation also contributed to the increasing surface area (Du et al. 2018a).

In terms of xCuCl$_2$/AC samples, both surface area and pore volume increased with the increasing content of CuCl$_2$, while the reverse occurred for the average pore diameter. As seen from SEM (Fig. 6), with higher loading value of CuCl$_2$, more active components entered into the pores, and more agglomerates were formed, thus causing the partial blockage of pores and then the decrease of average pore volume. And compared with 4.5% CuCl$_2$/AC, the growth of the flower-like structure into rod-like structure also led to a larger surface area for 5.7% CuCl$_2$/AC to a certain extent. Moreover, the minor increase of surface area caused by increasing CuCl$_2$ content accounted for the negligible increase of Hg^0 removal efficiency on xCuCl$_2$/AC at lower temperature, where physisorption closely related to surface area played a dominant role (Sun et al. 2017). Determined by multiple factors, the improvement of Hg^0 removal performance on xCuCl$_2$/AC at a higher temperature would be further discussed by the following characterizations.

XRD

The crystal structures of xCuCl$_2$/AC and virgin AC were characterized by XRD measurement, as depicted in Fig. 7. The SiO$_2$ diffraction peaks occurred at 2θ = 28.899°, 32.220°, and 36.040° and the diffraction lines for C at 60.086° were detected for virgin AC (Du et al. 2018a). After modified by CuCl$_2$, the characteristic peaks of AC were weakened obviously, suggesting the existence of interaction between AC and active components. For xCuCl$_2$/AC samples, the peak corresponding to CuCl$_2$·2H$_2$O was noted (Li et al. 2013a). With CuCl$_2$ content increasing, the peak became more intense and shifted to a higher binding energy. Moreover, two new peaks at 32.528° and 39.907° assigned to Cu$_2$(OH)$_3$Cl appeared on 4.5% CuCl$_2$/AC and 5.7% CuCl$_2$/AC, which was formed by the hydrolysis of CuCl$_2$·2H$_2$O, accounting for the shift of peak corresponding to CuCl$_2$·2H$_2$O (Liu et al. 2015). And Cu$_2$(OH)$_3$Cl was unstable at higher temperature, decomposing into CuCl$_2$ by losing hydroxyl groups (Leofanti et al. 2000), which was beneficial for the removal of Hg^0. The higher intensity of peaks appeared on 5.7% CuCl$_2$/AC indicated larger crystalline of active components, which was consistent with SEM.

XPS

In order to have a better research on Hg^0 removal mechanism, XPS measurement was carried out to indicate the chemical states of the surface elements.

Figure 8a showed the C 1s XPS spectra of fresh samples and treated 4.5% CuCl$_2$/AC. All samples included peaks attributed to graphic C (284.6–284.8 eV), carbon presenting in phenolic, alcohol or ether groups (285.8–286.0 eV), carbonyl or quinone groups (287.4–287.6 eV), carboxyl and ester groups (288.3–289.0 eV), and π-π* transitions in aromatic rings (290.2–290.6 eV), respectively (Zhou et al. 2007; Huang et al. 2017). It could be seen from Table 4, with the impregnation of CuCl$_2$, the graphic C decreased while the content of C bonded with O increased, suggesting the formation of more surface oxygen functional groups. And there was a positive correlation between the content of oxygen-contained functional groups, including C–O, C=O, COO–, and the loading value of CuCl$_2$. Thereinto, 5.7% CuCl$_2$/AC

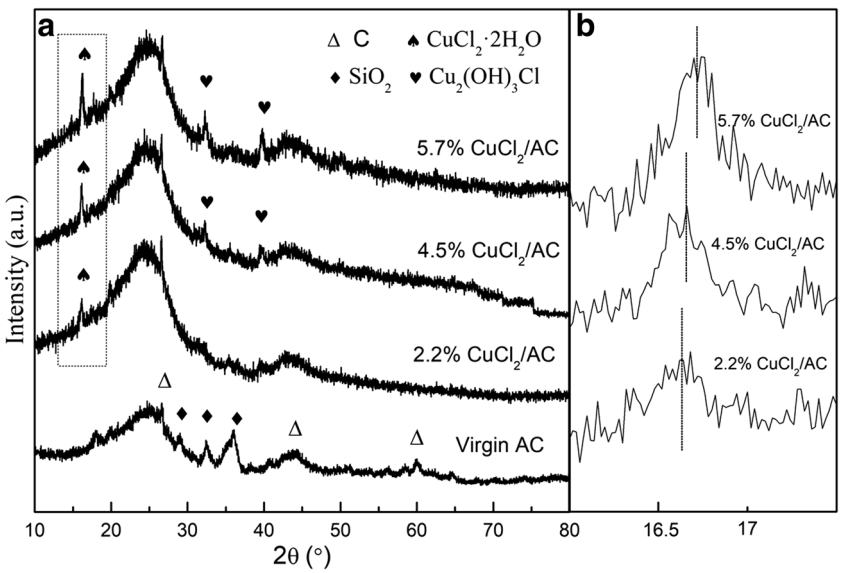

Fig. 7 XRD patterns of virgin AC, 2.2% CuCl$_2$/AC, 4.5% CuCl$_2$/AC, and 5.7% CuCl$_2$/AC

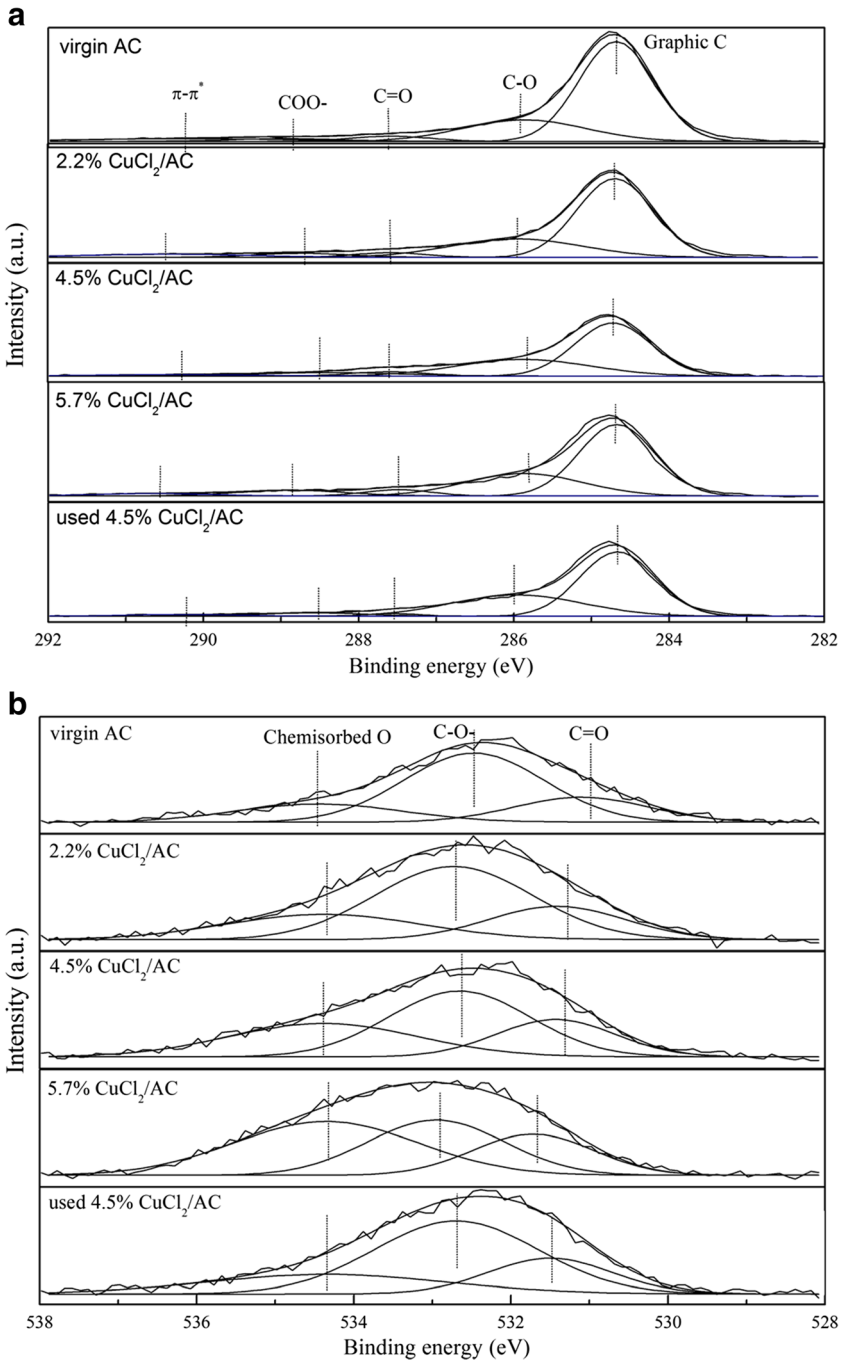

Fig. 8 XPS spectra of fresh and used virgin AC, 2.2% $CuCl_2$/AC, 4.5% $CuCl_2$/AC, and 5.7% $CuCl_2$/AC over the regions of **a** C 1s, **b** O 1s, **c** Cu 2p, **d** Hg 4f

possessed the highest content of C–O, C=O, COO–, which was 30.56%, 4.60%, and 7.04%, respectively. After treated with Hg^0, an obvious decrease was observed for both C=O and COO–, indicating the carbonyl and ester directly participated in the Hg^0 removal, and similar results were also found in other studies (Huang et al. 2017; Sun et al. 2017). These results agreed well with the highest removal and oxidation efficiency of 5.7% $CuCl_2$/AC whether there was with the presence of O_2 (Fig. 4). In a word, abundant surface oxygen-contained functional groups, particularly C=O and COO–, were beneficial for both adsorption and oxidation of Hg^0.

As displayed in Fig. 8b, the spectra of O 1s for all samples were fitted in three peaks at 531.1–531.5 eV, 532.4–533.0 eV, and 534.3–534.5 eV corresponding to the oxygen in carbonyl groups (C=O), the oxygen in alcohol or ether groups (C–O), and the chemisorbed oxygen, respectively (Biniak et al. 1997; Puziy et al. 2008). In comparison with virgin AC, the O 1s peaks of *x*$CuCl_2$/AC possessed higher binding energy, which might be due to the electron-transfer among O, C, and $CuCl_2$. Meanwhile, when $CuCl_2$ loading increased from 0 to 5.7%, both C=O and chemisorbed O rose simultaneously (Table 4), which was consistent with the tendency of removal activity. For used

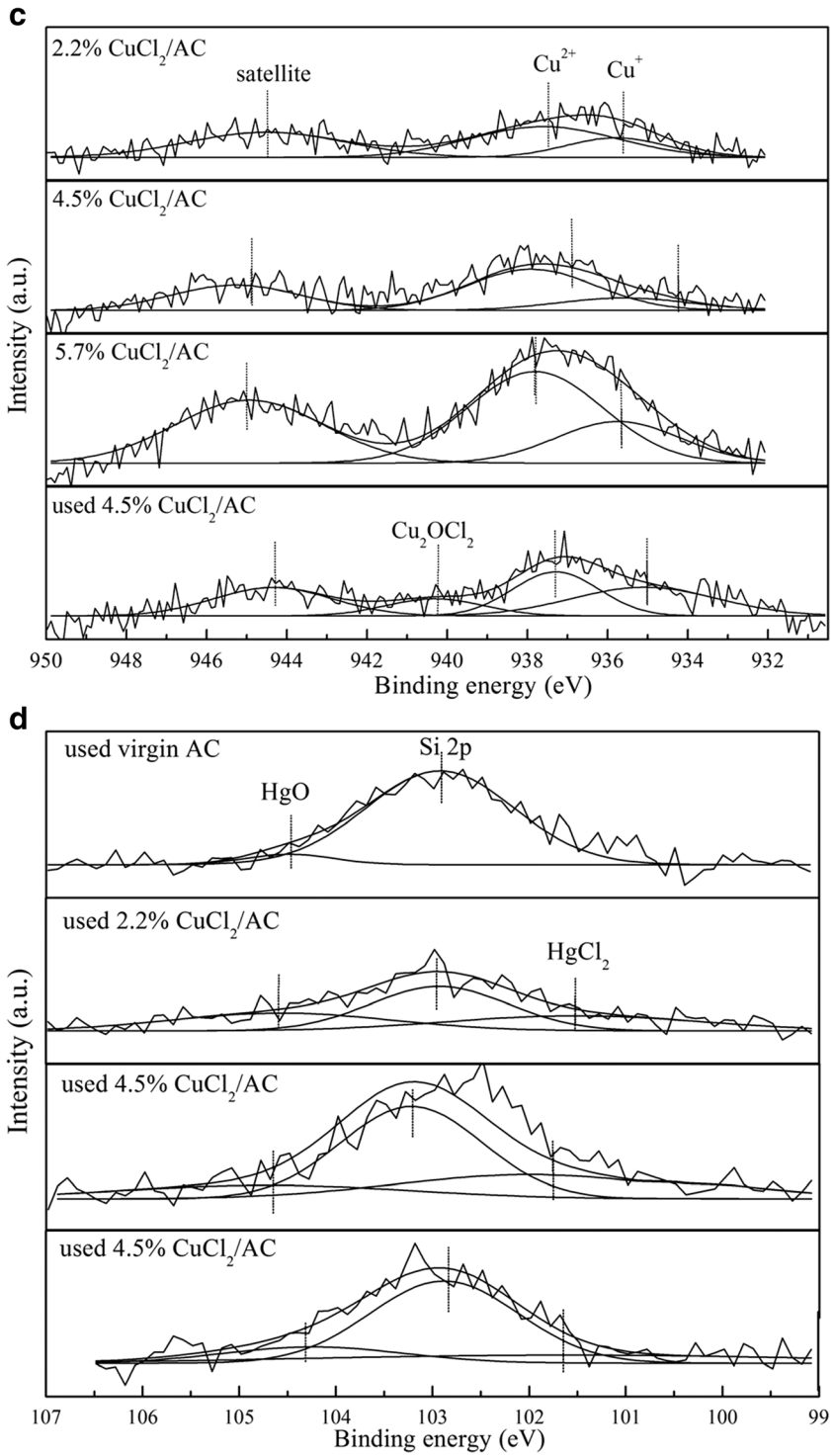

Fig. 8 continued.

4.5% $CuCl_2$/AC, both C=O and chemisorbed oxygen were consumed during Hg^0 removal. On one hand, C=O and chemisorbed O could act as the active sites for the Hg^0 adsorption and facilitate the adsorption of gaseous O_2. On the other hand, chemisorbed O could activate the lattice Cl of $CuCl_2$ and generate active chlorine species acting as the direct oxidant for Hg^0.

Figure 8c exhibited the spectra of Cu 2p, the peaks located at 934.9–935.9 eV were ascribed to Cu^+, the bands at 937.2–937.9 eV were assigned to Cu^{2+}, and the peaks of 944.2–945.3 eV contributed to the shake-up satellite. Notably, the peaks fitted in this work were with higher binding energy than other previous researches (Liu et al. 2015; Yang et al. 2016b),

Table 4 The relative XPS intensity of as-prepared samples

Relative intensity (%)	Virgin AC	2.2% $CuCl_2$/AC	4.5% $CuCl_2$/AC	5.7% $CuCl_2$/AC	Used 4.5% $CuCl_2$/AC
Graphic C	65.45	61.30	57.76	55.04	58.05
C–O	23.32	25.48	28.08	30.56	33.69
C=O	3.79	3.68	4.49	4.60	1.73
COO–	2.82	4.22	6.81	7.04	4.33
π-π^*	4.62	5.32	2.86	2.76	2.20
C=O	20.87	21.61	22.16	22.26	20.99
C–O–	60.19	54.80	46.41	33.74	56.69
Chemisorbed O	18.94	23.59	31.43	44.00	22.32
[a]Cu^+	–	18.61	16.06	19.07	31.83
[a]Cu^{2+}	–	43.43	51.83	46.13	29.27
[a]Satellite	–	37.96	32.11	34.80	26.01
[a]Cu_2OCl_2	–	–	–	–	12.89
[a]Cu^{2+}/Cu^+	–	2.33	3.23	2.42	0.92
[b]Hg^0	6.13	28.20	16.01	15.78	–
[b]$HgCl_2$	–	27.18	26.92	18.01	–

[a] The percent of different valence of Cu in Cu $2p_{3/2}$

[b] The relative intensity of $Hg^0/(Hg^0 + HgCl_2 + Si\ 2p)$ or $HgCl_2/(Hg^0 + HgCl_2 + Si\ 2p)$ over the sample after treating with 70 μg/m^3 Hg^0 + 6% O_2

which might be due to the different chemical environment of Cu atoms over different support. For *x*$CuCl_2$/AC samples, the ratio of Cu^{2+}/Cu^+ followed the following sequence: 4.5% $CuCl_2$/AC > 5.7% $CuCl_2$/AC > 2.2% $CuCl_2$/AC. Higher content of Cu^{2+} could provide not only more Cu sites for Hg^0 adsorption, but also more active Cl to oxidize Hg^0. And the ratio of Cu^{2+}/Cu^+ of fresh 4.5% $CuCl_2$/AC decreased sharply from 3.23 to 0.92 after the treatment with Hg^0, indicating the existence of redox reaction $CuCl_2 \leftrightarrow CuCl$ during Hg^0 removal. It was worth mentioning that the peak corresponding to Cu_2OCl_2 was found over used 4.5% $CuCl_2$/AC, which was formed by the reaction $2\ CuCl + 1/2\ O_2 \rightarrow Cu_2OCl_2$ (Leofanti et al. 2002). Besides, Cu_2OCl_2 could be converted to $CuCl_2$ with the aid of HCl, and the promotion effect of HCl in the "Effect of O_2 and HCl" section could be explained.

The Hg 4f spectra of the used samples are displayed in Fig. 8d. The peaks at 104.2–104.6 eV, around 102.9 eV and 101.5 eV, were for Hg^0, Si 2p, and $HgCl_2$, respectively (Ma et al. 2015). Only Hg^0 with the content of 6.13% was detected over used virgin AC, indicating the chemisorption of Hg^0 could proceed by means of abundant active oxygen species, including chemisorbed O and surface oxygen-contained functional species, which was testified by the XPS characterization results of C1s and O 1s. Besides Hg^0, $HgCl_2$ was also found over AC impregnated with $CuCl_2$. In combination with the O 1s (Fig. 8b) and Cu 2p spectra (Fig. 8c), the reaction $Hg^0 + 2CuCl_2 + O^* \rightarrow HgCl_2 + 2CuCl + O$ was confirmed. Besides, the content of Hg^{2+} species (Hg^0 and $HgCl_2$) on the surface of used samples reduced from 55.38% to 42.93% and 33.79% with the increasing loading value. This might be with higher $CuCl_2$ loading, the chemisorption dropped off, and the catalytic oxidation was enhanced, which was in accordance with mercury conversion experiment.

Moreover, XPS and Hg-TPD were also carried out to investigate the promotion effect of SO_2 and NO on Hg removal over 4.5% $CuCl_2$/AC. As depicted in Fig. 9 and Table 5, compared with 4.5% $CuCl_2$/AC, an obvious increase for C–O and decrease for chemisorbed O were observed for both used (+NO) 4.5% $CuCl_2$/AC and used (+SO_2) 4.5% $CuCl_2$/AC samples, indicating the consumption of chemisorbed O during Hg^0 removal. And the reduction of $Cu^{2+} \rightarrow Cu^+$ also occurred to provide more active oxygen for Hg^0 removal with the presence of SO_2 and NO. Moreover, a higher Cu_2OCl_2 content was observed for both used (+NO) 4.5% $CuCl_2$/AC and used (+SO_2) 4.5% $CuCl_2$/AC than used 4.5% $CuCl_2$/AC. As reported, Cu_2OCl_2 possessed a better Hg^0 removal capacity than CuCl, and then contributed to the sample with a higher activity, which accounted for the promotion effect of NO and SO_2 to some extent (Yang et al. 2016b). Notably, used (+NO) 4.5% $CuCl_2$/AC possessed a larger Cu^{2+}/Cu^+ than used 4.5% $CuCl_2$/AC, which might be due to the formation of NO_2 and acted as oxidant for Hg^0, thus decelerating the reduction of Cu^{2+}. In terms of S, the addition of SO_2 into simulated flue gas resulted in an increase of 32.63% for S^{6+}, including SO_4^{2-} and HSO_4^- (Liao et al. 2016). And there was a slight shift of peaks ascribed to Hg^{2+} when adding NO and SO_2 into simulated flue gas, and it might be due to the bond between Hg atoms with NO_3^- or SO_4^{2-} (Zhao et al. 2016a).

As displayed in Fig. 10, the TPD profile of used 4.5% $CuCl_2$/AC was fitted into two peaks located at 287 and 321

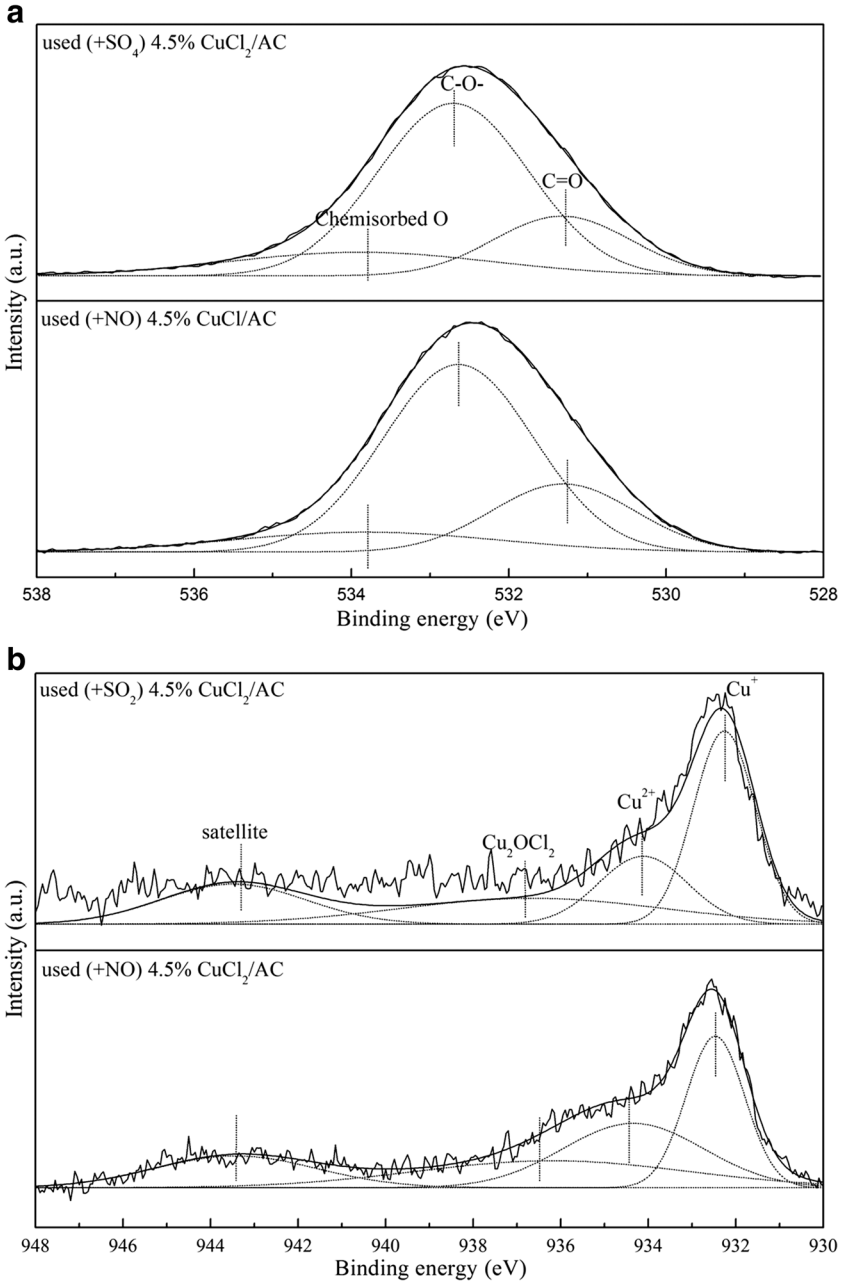

Fig. 9 XPS spectra of used 4.5% $CuCl_2$/AC, used (+NO) 4.5% $CuCl_2$/AC and used (+SO_2) 4.5% $CuCl_2$/AC over the regions of **a** O 1s, **b** Cu 2p, **c** Hg 4f, **d** S 2p

°C, which was ascribed to the desorption of $HgCl_2$ and Hg^0, respectively (Zhang et al. 2017a, b), which was consistent with the XPS results of Hg 4f. Besides the peak relevant to $HgCl_2$ and Hg^0, an additional peak ascribed to the desorption of $Hg(NO_3)_2$ appeared at 418 °C for used (+NO) 4.5% $CuCl_2$/AC. The generation of $Hg(NO_3)_2$, through the reaction $Hg^0 + O^* + NO/NO_2 \rightarrow Hg(NO_3)_2$, contributed to the enhanced Hg^0 removal efficiency with NO_2, which verified the assumption in the "Effect of SO2 and NO" section (Rumayor et al. 2015). In terms of used (+SO_2) 4.5% $CuCl_2$/AC, the peak attributed to $HgCl_2$ and Hg^0 shifted to a lower temperature. In accordance with the S 2p and Hg 4f (Fig. 9), the generation of $HgSO_4$ was further confirmed by the desorption peak of $HgSO_4$ at 445 °C (Zhang et al. 2017b).

FT-IR

To analyze the change of surface oxygen functional groups and intermediates during Hg^0 removal process, FT-IR characterization at 500–4000 cm^{-1} was conducted for fresh and used samples, respectively. As depicted from Fig. 11, compared with virgin AC, the peaks at 3370 and 3450 cm^{-1} assigned

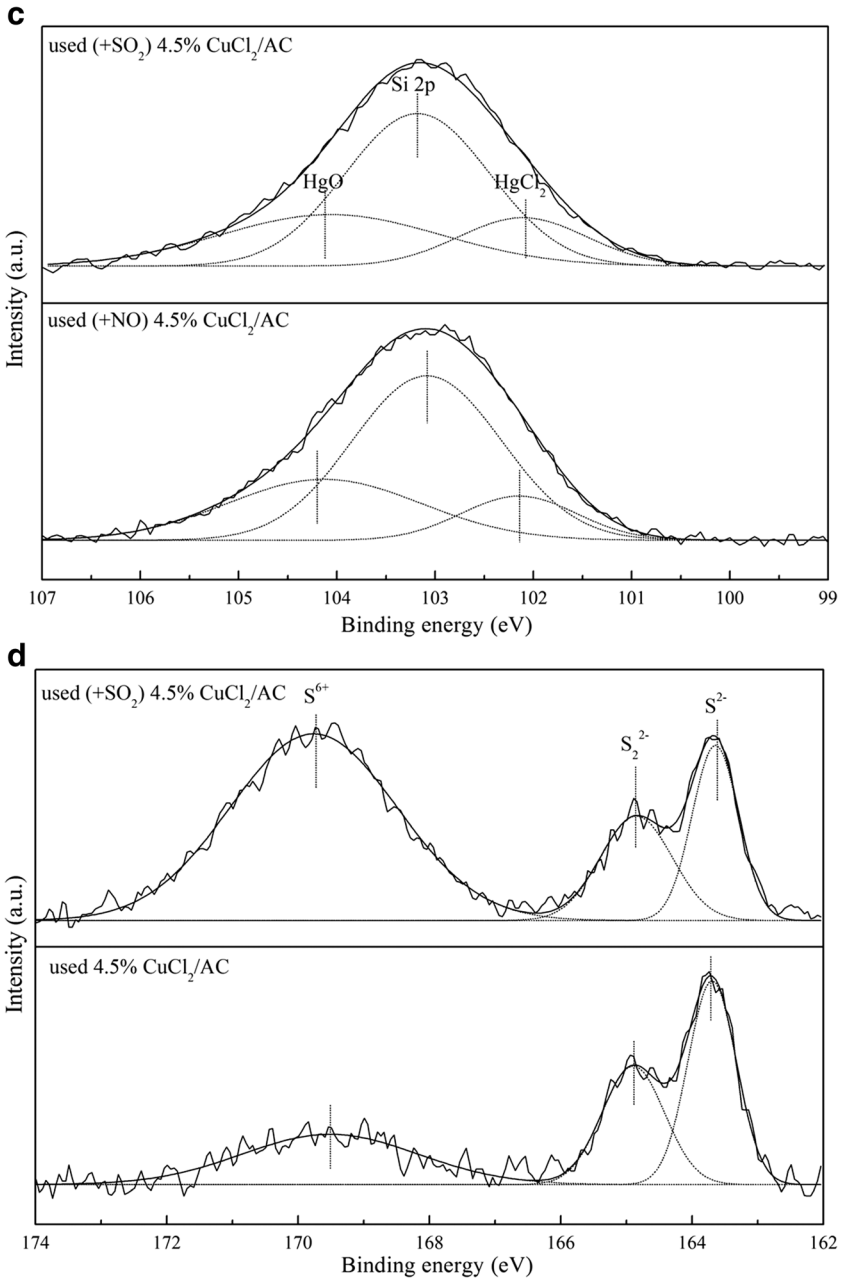

Fig. 9 continued.

to the v_s(OH) were observed on fresh modified AC (Leofanti et al. 2000), and its intensity increased with the increasing loading of $CuCl_2$. And the formation of –OH contributed to the increase of chemisorbed O, which was consistent with the tendency of chemisorbed O in Fig. 8b. As reported, $Cu_2(OH)_3Cl$ would be decomposed into $CuCl_2$ at elevated temperature, and –OH was formed during the process (Liu et al. 2015). And hydroxyl group would facilitate the Hg^0 removal through ligand exchange (Huang et al. 2017). After the treatment with Hg^0, the peaks of –OH was weakened, suggesting the participation of hydroxyl in Hg^0 removal. Besides, the characteristic peaks of C at 2320 and 2375 cm^{-1} were also found for $xCuCl_2$/AC with a weakened intensity, confirming the interaction between AC and $CuCl_2$, as described in XRD and XPS. Peaks at 1000–1200 cm^{-1} were contributed to v_s(C–O) and v_s(C–OH) in alcohol or ether groups (González-Elipe et al. 1988), and were endowed a higher intensity after the dopant of $CuCl_2$, which was consistent with the XPS characterizations.

Mechanism discussion

As seen from the experimental results, with the dopant of $CuCl_2$, a great improvement in Hg^0 removal occurred

Table 5 The relative XPS intensity of 4.5% $CuCl_2$ treated under different atmospheres

Relative intensity (%)	Used 4.5% $CuCl_2$/AC	Used (+NO) 4.5% $CuCl_2$/AC	Used (+SO_2) 4.5% $CuCl_2$/AC
C=O	–	22.48	20.18
C–O–	–	65.35	64.48
Chemisorbed O	–	12.17	15.34
[a]Cu^+	–	29.39	39.25
[a]Cu^{2+}	–	29.90	19.69
[a]Cu_2OCl_2	–	23.76	22.06
[a]Satellite	–	16.94	19.00
[b]$HgCl_2$	–	12.36	15.67
[b]Hg^0	–	28.48	28.65
S^{2-}	37.71	–	17.41
S_2^{2-}	28.36	–	16.03
S^{6+}	33.93	–	66.56

[a] The percent of different valence of Cu in Cu $2p_{3/2}$

[b] The relative intensity of Hg^0 /(Hg^0 + $HgCl_2$ + Si 2p) or $HgCl_2$/(Hg^0 + $HgCl_2$ + Si 2p) over the sample after the treatment

for AC. Besides, AC modified with $CuCl_2$ exhibited superior Hg^0 removal performance at a broader temperature range. On one hand, the flower-like or rod-like structure formed on the $x$$CuCl_2$/AC owing to the impregnation of $CuCl_2$ enlarged the BET surface area, thus providing more active sites for both adsorption and oxidation of gas reactants. And the XRD characterization indicated that the $CuCl_2$ existed in the forms of $CuCl_2 \cdot 2H_2O$ and $Cu_2(OH)_3Cl$. On the other hand, $x$$CuCl_2$/AC possessed abundant surface oxygen functional groups, especially for carbonyl and ester groups, as well as chemisorbed oxygen and –OH. It could not only act as active sites for the adsorption of Hg^0 and O_2, but also activate lattice Cl and form active chlorine to oxidize Hg^0 directly. Remarkably, the higher content of oxygen-contained functional groups and chemisorbed O led to a higher oxidation efficiency of Hg^0. Besides, a higher Cu^{2+} content facilitated the Hg^0 removal via providing more Cu sites and Cl sites for adsorption and oxidation.

Basing on the above experimental and characterization results, Hg^0 removal mechanism on $x$$CuCl_2$/AC was proposed in Fig. 12. Firstly, the gas-phase Hg^0 adsorbed on the active sites of sample, including Cu sites, Cl sites, and surface

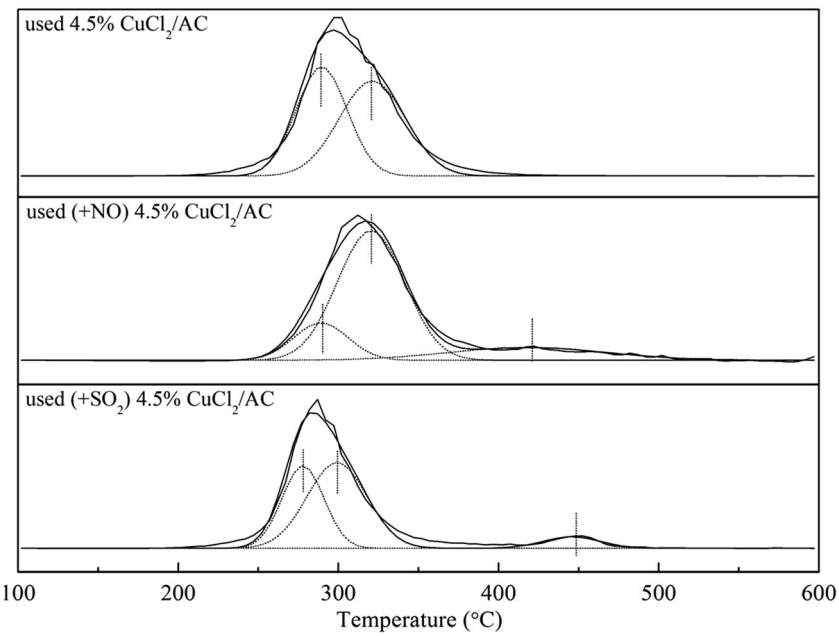

Fig. 10 Hg-TPD profiles of 4.5% $CuCl_2$/AC, used (+NO) 4.5% $CuCl_2$/AC, and used (+SO_2) 4.5% $CuCl_2$/AC

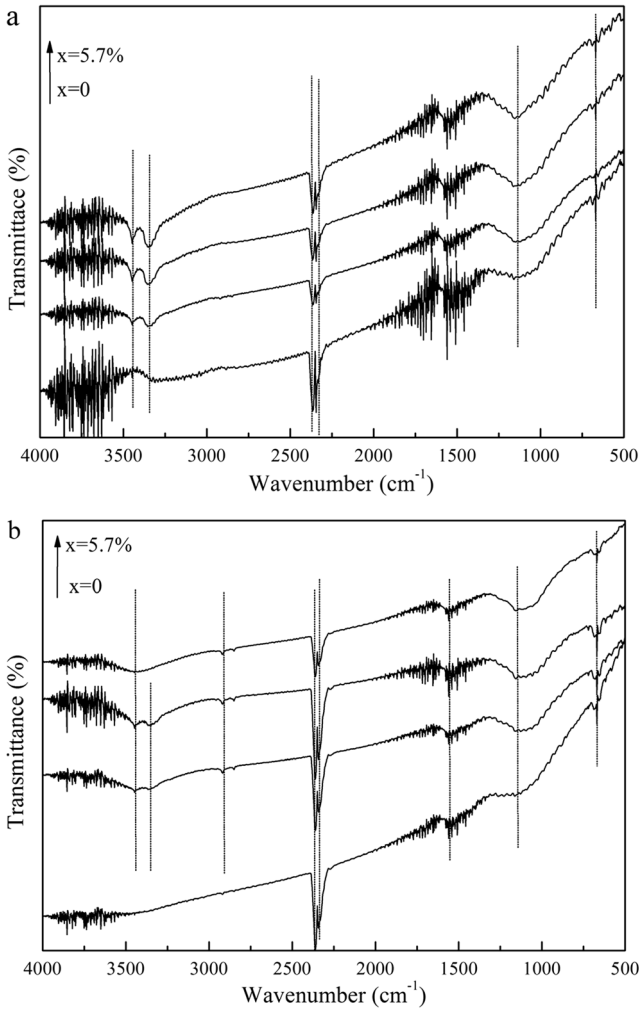

Fig. 11 FT-IR spectra of **a** fresh and **b** used virgin AC, 2.2% $CuCl_2$/AC, 4.5% $CuCl_2$/AC, and 5.7% $CuCl_2$/AC from bottom to top (reaction condition 0.05 g sample, 6% O_2, 70 μg/m^3 Hg^0, N_2 as balance gas, T = 140 °C, total flow rate 500 mL/min, reaction time 240 min)

functional groups, and formed $Hg^0_{(ads)}$. Then, in combination with XPS and FT-IR characterization results, a part of $Hg^0_{(ads)}$ was oxidized by the active oxygen (O^*), such as surface oxygen functional groups, chemisorbed O and –OH, and converted into $Hg^0_{(ads)}$. What's more, O^* also could activate lattice Cl of $CuCl_2$, which was produced by the decomposition of $Cu_2(OH)_3Cl$ under elevated temperature, and the formed active Cl (Cl^*) combined with $Hg^0_{(ads)}$. In this reaction, $Hg^0_{(ads)}$ was oxidized into $HgCl_{2(ads)}$ or $HgCl_{(ads)}$ and $CuCl_2$ was converted into CuCl after losing Cl. Besides, the formed CuCl could be oxidized into Cu_2OCl_2 by gaseous O_2. And the consumed O^* was supplemented by gaseous O_2. Finally, a small amount of $Hg^0_{(ads)}$ and $HgCl_{2(ads)}$ desorbed from the surface of $x$$CuCl_2$/AC, which could be testified by the mercury conversion experiment. Therefore, the chemisorption was the predominant approach of Hg^0 removal on $x$$CuCl_2$/AC, and the above reaction could be described as follows:

$$Hg^0_{(g)} \rightarrow Hg^0_{(ads)} \quad (5)$$

$$Hg^0_{(ads)} + O^* \rightarrow HgO_{(ads)} \quad (6)$$

$$CuCl_2 \rightarrow^{O^*} CuCl + Cl^* \quad (7)$$

$$Hg^0_{(ads)} + Cl^* \rightarrow HgCl \quad (8)$$

$$HgCl + Cl^* \rightarrow HgCl_2 \quad (9)$$

$$4CuCl + O_2 \rightarrow 2Cu_2OCl_2 \quad (10)$$

$$O_2 \rightarrow 2O^* \quad (11)$$

$$HgO_{(ads)} \rightarrow Hg0_{(g)} \quad (12)$$

$$HgCl_{2(ads)} \rightarrow HgCl_{2(g)} \quad (13)$$

Simulated industrial application test

To investigate the Hg^0 removal performance of $CuCl_2$-modified CAC in industrial application, simulated industrial application test was conducted. As depicted in Fig. 13, initial Hg^0 removal efficiency of 69.00%, 81.29%, and 85.26% was reached at 140 °C for CAC, CAC-3, and CAC-8, respectively. The improvement of Hg^0 removal efficiency after regeneration might be contributed to two aspects. On one hand, the generation of new micropores due to the formed sulfur-contained species during regeneration process would increase the BET surface area and pore volume, which could facilitate the adsorption of Hg^0 on the surface of AC (Ma et al. 2015). On the other hand, SO_4^{2-} and SO_3^{2-} formed could act as the active sites for Hg^0 removal, through S-bonded chemisorption, to form $HgSO_4$ and $HgSO_3$, which has been discussed in the "Effect of SO2 and NO" section 3.2.2. However, a sharp decline was also observed with the reaction time increasing. Notably, with the impregnation of $CuCl_2$, a dramatic increase over 60% was achieved for all three samples after reacted for 22 h. Combining the bench-scale test with simulated industrial application test, $CuCl_2$/AC has the huge potential in efficient removal of Hg^0 in the multi-pollutant removal system with AC. And further study concerning the practical application and the mechanism on the regeneration of AC will be carried out.

Conclusion

$x$$CuCl_2$/AC samples with different $CuCl_2$ loading prepared by impregnation method were investigated on elemental mercury removal on a fixed bed. $x$$CuCl_2$/AC possessed excellent Hg^0 removal efficiency higher than 90% at 80–140 °C, even higher than 95% for 4.5% $CuCl_2$/AC and 5.7% $CuCl_2$/AC.

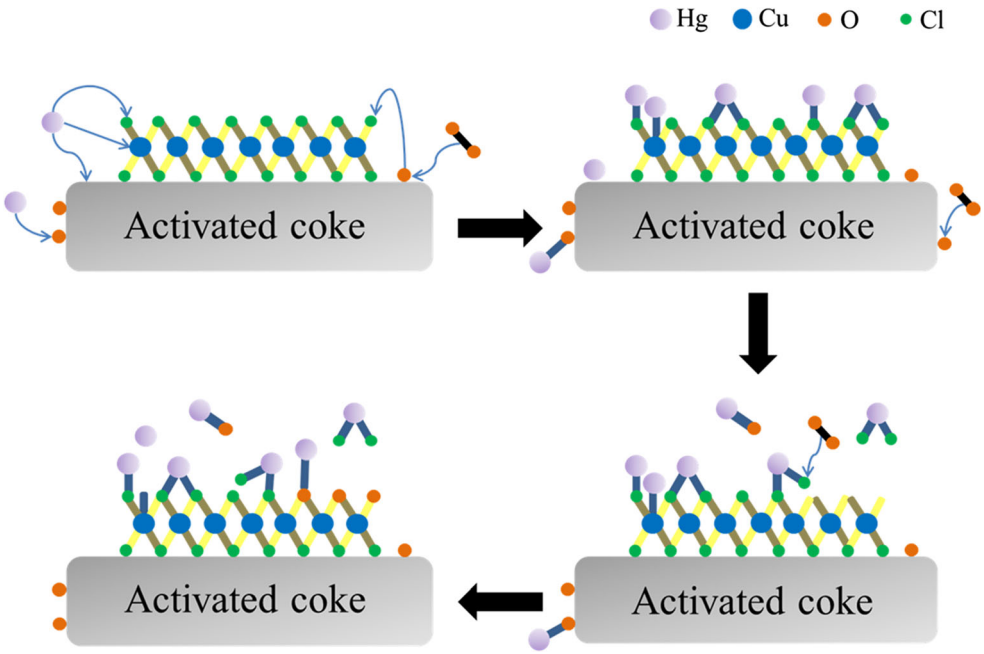

Fig. 12 The proposed mechanism of Hg^0 removal on $xCuCl_2$/AC

Besides, O_2 promoted the Hg^0 removal significantly through the replenishment of O^* consumed in Hg^0 removal, and only 2% O_2 could meet the need of Hg^0 removal in this study. Both SO_2 and NO played a positive effect on Hg^0 removal on account of the formation of $HgSO_4$ and $Hg(NO_3)_2$, and the promotion effect was further strengthened by the addition of O_2. Moreover, numerous characterizations, such as SEM, BET, XRD, XPS, and FT-IR, were carried out to investigate the physiochemical properties of both AC and modified AC. The excellent performance of $xCuCl_2$/AC could be contributed to the higher BET surface area, abundant surface oxygen-contained functional groups and chemisorbed oxygen, and higher Cu^{2+} content. Based on above researches, the mechanism of Hg^0 removal on $xCuCl_2$/AC was proposed. On one hand, Hg^0 was oxidized by surface active oxygen and formed Hg^0. On the other hand, the lattice Cl was activated by active oxygen into active chlorine, and then oxidized Hg^0 into $HgCl_2$. In addition, a small amount of Hg^{2+} monitored in outlet flue gas manifested that the catalytic oxidation participated in the Hg^0 removal besides adsorption. During the process, Cu_2OCl_2, which could be recovered to $CuCl_2$ with the aid of HCl, was also observed as an intermediate on samples. Moreover, $xCuCl_2$/AC was proved to maintain its high activity after 36-h stability test. And simulated industrial application test on Hg^0 removal using virgin and regenerated columnar AC modified with $CuCl_2$ spray solution was also conducted for 22 h, exhibiting its potential in practical industry application.

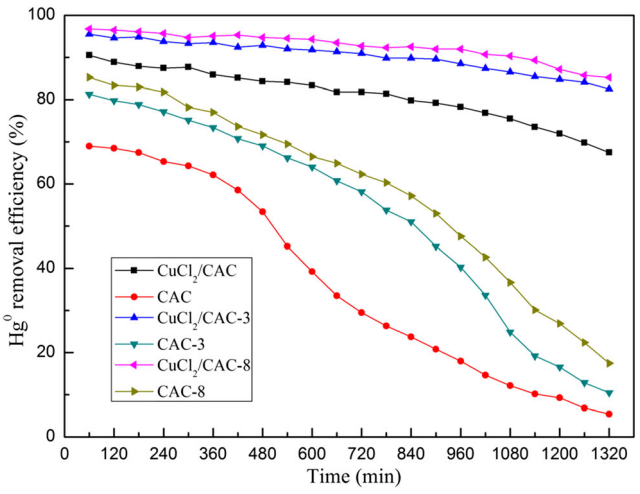

Fig. 13 The simulated industrial application test of $CuCl_2$-modified fresh and regenerated CAC (reaction condition 50 g sample, 6% O_2, 70 μg/m^3 Hg^0, 400 ppm SO_2, 500 ppm NO, N_2 as balance gas, T = 140 °C, total flow rate 500 mL/min)

Funding information This study was supported by the National Key research and Development Program of China (2016YFC0204100).

References

Abrishamkar M, Kahkeshi FB (2013) Synthesis and characterization of nano-ZSM-5 zeolite and its application for electrocatalytic oxidation of formaldehyde over modified carbon paste electrode with ion exchanged synthesized zeolite in alkaline media. Microporous Mesoporous Mater 167:51–54

Aissat A, Courcot D, Cousin R, Siffert S (2011) VOCs removal in the presence of NO_x on Cs–Cu/ZrO_2 catalysts. Catal Today 176:120–125

Biniak S, Szymański G, Siedlewski J, Świątkowski (1997) The characterization of activated carbons with oxygen and nitrogen surface groups. Carbon 35(12):1799–1810

Cao Y, Chen B, Wu J, Cui H, Smith J, Chen C, Chu P, Pan P (2007) Study of mercury oxidation by a selective catalytic reduction catalyst in a

pilot-scale slipstream reactor at a utility boiler burning bituminous coal. Energy Fuel 21:145–156

Du X, Li C, Zhao L, Zhang J, Gao L, Sheng J, Yi Y, Chen J, Zeng G (2018a) Promotional removal of HCHO from simulated flue gas over Mn-Fe oxides modified activated coke. Appl Catal B Environ 232:37–48

Du J, Qu Z, Dong C, Song L, Qin Y, Huang N (2018b) Low-temperature abatement of toluene over Mn-Ce oxides catalysts synthesized by a modified hydrothermal approach. Appl Surf Sci 433:1025–1035

Fan X, Li C, Zeng G, Zhang X, Tao S, Lu P, Tan Y, Luo D (2012) Hg^0 removal from simulated flue gas over CeO_2/HZSM-5. Energy Fuel 26:2082–2089

Fuente-Cuesta A, Lopez-Anton MA, Diaz-Somoano M, Martínez-Tarazona MR (2012) Retention of mercury by low-cost sorbents: influence of flue gas composition and fly ash occurrence. Chem Eng J 213:16–21

Ghorishi SB, Singer CF, Jozewicz WS, Sedman CB, Srivastava (2011) Simultaneous control of Hg^0, SO_2, and NO_x by novel oxidized calcium-based sorbents. J Air Waste Manage 52:273–278

González-Elipe AR, Martínez-Alonso A, Tascón JM (1988) XPS characterization of coal surfaces: study of aerial oxidation of brown coals. Surf Interface Anal 12:565–571

Granite EJ, Pennline HW, Hargis HW (2000) Novel sorbents for mercury removal from flue gas. Ind Eng Chem Res 39:1020–1029

Granite EJ, Freeman MC, Hargis RA, O'Dowd WJ, Pennline HW (2007) The thief process for mercury removal from flue gas. J Environ Manag 84:628–634

He S, Zhou J, Zhu Y, Luo Z, Ni M, Cen K (2009) Mercury oxidation over a vanadia-based selective catalytic reduction catalyst. Energy Fuel 23:253–259

He C, Shen B, Chen J, Cai J (2014) Adsorption and oxidation of elemental mercury over Ce-MnOx/Ti-PILCs. Environ Sci Technol 48: 7891–7898

He C, Shen B, Chi G, Li F (2016) Elemental mercury removal by CeO2/TiO2-PILCs under simulated coal-fired flue gas. Chem Eng J 300: 1–8

Hsi HC, Tsai CY (2012) Synthesis of TiO_{2-x} visible-light photocatalyst using N_2/Ar/He thermal plasma for low-concentration elemental mercury removal. Chem Eng J 191:378–385

Huang Y, Tang J, Gai L, Gong Y, Guan H, He R, Lyu H (2017) Different approaches for preparing a novel thiol-functionalized graphene oxide/Fe-Mn and its application for aqueous methylmercury removal. Chem Eng J 319:229–239

Jeong SM, Jung SH, Yoo KS, Kim SD (1999) Selective catalytic reduction of NO by NH_3 over a bulk sulfated CuO/γ-Al_2O_3 catalyst. Ind Eng Chem Res 38:2210–2215

Jin R, Wu Z, Wang H, Gu T (2010) Low-temperature selective catalytic reduction of NO with NH_3 over Mn-Ce oxides supported on TiO_2 and Al_2O_3: a comparative study. Chemosphere 78:1160–1166

Kan J, Deng L, Li B, Huang Q, Zhu S, Shen S, Chen Y (2017) Performance of co-doped Mn-Ce catalysts supported on cordierite for low concentration chlorobenzene oxidation. Appl Catal A Gen 530:21–29

Kim MH, Ham SW, Lee JB (2010) Oxidation of gaseous elemental mercury by hydrochloric acid over $CuCl_2$/TiO_2-based catalysts in SCR process. Appl Catal B Environ 99:272–278

Leofanti G, Padovan M, Garilli M, Carmello D, Marra GL, Zecchina A, Spoto G, Bordiga S, Lamberti C (2000) Alumina-supported copper chloride. J Catal 189:105–116

Leofanti G, Marsella A, Cremaschi B, Garilli M, Zecchina A, Spoto G, Bordiga S, Fisicaro P, Prestipino C, Villain F, Lamberti C (2002) Alumina-supported copper chloride. J Catal 205:375–381

Li Y, Lee C, Gullett B (2003) Importance of activated carbon's oxygen surface functional groups on elemenal mercury adsorption. Fuel 82: 451–457

Li H, Li Y, Wu C, Zhang J (2011a) Oxidation and capture of elemental mercury over SiO_2–TiO_2–V_2O_5 catalysts in simulated low-rank coal combustion flue gas. Chem Eng J 169:186–193

Li H, Wu C, Li Y, Zhang J (2011b) CeO_2-TiO_2 catalysts for catalytic oxidation of elemental mercury in low-rank coal combustion flue gas. Environ Sci Technol 45:7394–7400

Li H, Wu C, Li Y, Zhang Y (2012) Superior activity of MnO_x-CeO_2/TiO_2 catalyst for catalytic oxidation of elemental mercury at low flue gas temperatures. Appl Catal B Environ 111-112:381–388

Li X, Liu Z, Kim J, Lee JY (2013a) Heterogeneous catalytic reaction of elemental mercury vapor over cupric chloride for mercury emissions control. Appl Catal B Environ 132-133:401–407

Li X, Liu Z, Lee JY (2013b) Adsorption kinetic and equilibrium study for removal of mercuric chloride by $CuCl_2$-impregnated activated carbon sorbent. J Hazard Mater 252-253:419–427

Li H, Wu C, Li Y, Zhang Y (2013c) Impact of SO_2 on elemental mercury oxidation over CeO_2–TiO_2 catalyst. Chem Eng J 219:319–326

Liao Y, Chen D, Zou S, Xiong S, Xiao X, Dang H, Chen T, Yang S (2016) Recyclable naturally derived magnetic pyrrhotite for elemental mercury recovery from flur gas. Environ Sci Technol 50:10562–10569

Liu Z, Li X, Lee JY, Bolin TB (2015) Oxidation of elemental mercury vapor over γ-Al_2O_3 supported $CuCl_2$ catalyst for mercury emissions control. Chem Eng J 275:1–7

Ma J, Li C, Zhao L, Zhang J, Song J, Zeng G, Zhang X, Xie Y (2015) Study on removal of elemental mercury from simulated flue gas over activated coke treated by acid. Appl Surf Sci 329:292–300

Niksa S, Fujiwara N (2005) A predictive mechanism for mercury oxidation on selective catalytic reduction catalysts under coal-derived flue gas. J Air Waste Manage Assoc 55:1866–1875

Norton GA, Yang H, Brown RC, Laudal DL, Dunham GE, Erjavec J (2003) Heterogeneous oxidation of mercury in simulated post combustion conditions. Fuel 82:107–116

Pavlish JH, Hamre LL, Zhuang Y (2010) Mercury control technologies for coal combustion and gasfication systems. Fuel 89:838–847

Presto AA, Granite EJ (2006) Survey of catalysts for oxidation of mercury in flue gas. Environ Sci Technol 40(18):5601–5609

Puziy AM, Poddubnaya OI, Socha RP, Gurgul J, Wisniewski M (2008) XPS and NMR studies of phosphoric acid activated carbons. Carbon 46:2113–2123

Qu W, Yang Y, Shen F, Yang J, Fang S, Li H (2018) Theoretical study on Hg^0 adsorption and oxidation mechanisms over $CuCl_2$-impregnated carbonaceous material surface. Energy Fuel 32:7125–7131

Rumayor M, Miranda N, Anton M, Somoano M, Tarazona M (2015) Application of mercury temperature programmed desorption (HgTPD) to ascertain mercury/char interactions. Fuel Process Technol 132:9–14

Senior CL (2012) Oxidation of mercury across selective catalytic reduction catalysts in coal–fired power plants. J Air Waste Manage Assoc 56:23–31

Sheng J, Li C, Zhao L, Gao L, Zeng G (2017) Efficient removal of HCHO from simulated coal combustion flue gas using CuO-CeO_2 supported on cylindrical activated coke. Fuel 197:397–406

Sjostrom S, Durham M, Bustard CJ, Martin C (2010) Activated carbon injection for mercury control: overview. Fuel 89:1320–1322

Streets DG, Devane MK, Lu Z, Bond TC, Sunderland EM, Jacob DJ (2011) All-time releases of mercury to the atmosphere from human activities. Environ Sci Technol 45:10485–10491

Sun P, Zhang B, Zeng X, Luo G, Li X, Yao H, Zheng C (2017) Deep study on effects of activated carbon's oxygen functional groups for elemental mercury adsorption using temperature programmed desorption method. Fuel 200:100–106

Tan Z, Su S, Qiu J, Kong F, Wang Z, Hao F, Xiang J (2012) Preparation and characterization of Fe_2O_3–SiO_2 composite and its effect on elemental mercury removal. Chem Eng J 195-196:218–225

Tang L, Li C, Zhao L, Gao L, Du X, Zeng J, Zhang J, Zeng G (2018) A novel catalyst CuO-ZrO_2 doped on Cl^- activated bio-char for Hg^0 removal in a broad temperature range. Fuel 218:366–374

Tao S, Li C, Fan X, Zeng G, Lu P, Zhang X, Wen Q, Zhao W, Luo D, Fan C (2012) Activated coke impregnated with cerium chloride used for elemental mercury removal from simulated flue gas. Chem Eng J 210:547–556

Tsuji K, Shiraishi I (1990) Combined desulfurization and denitrification and reduction of air toxics using activated coke 1: activity of activated coke. Fuel 76:549–553

Tsuji K, Shiraishi I (1997) Combined desulfurization, denitrification and reduction of air toxics using activated coke 2: process application and performance of activated coke. Fuel 76:555–560

Wang Y, Liu Y, Wu Z, Mo J, Cheng B (2010) Experimental study on the absorption behaviors of gas phase bivalent mercury in Ca-based wet flue gas desulfurization slurry system. J Hazard Mater 183:902–907

Wang P, Su S, Xiang J, Cao F, Sun L, Hu S, Lei S (2013) Catalytic oxidation of Hg^0 by CuO–MnO_2–Fe_2O_3/γ-Al_2O_3 catalyst. Chem Eng J 225:68–75

Wang Y, Li C, Zhao L, Xie Y, Zhang X, Zeng G, Wu H, Zhang J (2016) Study on the removal of elemental mercury from simulated flue gas by Fe_2O_3-CeO_2/AC at low temperature. Environ Sci Pollut Res 23: 5099–5110

Wu H, Li C, Zhao L, Zhang J, Zeng G, Xie Y, Zhang X, Wang Y (2015) Removal of gaseous elemental mercury by cylindrical activated coke loaded with CoO_x-CeO_2 from simulated coal combustion flue gas. Energy Fuel 29:6747–6757

Wu Q, Wang S, Li G, Liang S, Lin C, Wang Y, Cai S, Liu K, Hao J (2016) Temporal trend and spatial distribution of speciated atmospheric mercury emissions in China during 1978-2014. Environ Sci Technol 50:13428–13435

Wu J, Zhao Z, Huang T, Zhang J, Tian H, Zhao X, Zhao L, He P, Ren J, Gao K (2017) Removal of elemental mercury by Ce-Mn co-modified activated carbon catalyst. Catal Commun 93:62–66

Yang H, Xu Z, Fan M, Bland AE, Judkins RR (2007) Adsorbents for capturing mercury in coal-fired boiler flue gas. J Hazard Mater 146: 1–11

Yang J, Zhao Y, Zhang J, Zheng C (2016a) Removal of elemental mercury from flue gas by recyclable $CuCl_2$ modified magnetospheres catalyst from fly ash. Part 1. Catalyst characterization and performance evaluation. Fuel 164:419–428

Yang J, Zhao Y, Zhang J, Zheng C (2016b) Removal of elemental mercury from flue gas by recyclable $CuCl_2$ modified magnetospheres catalyst from fly ash. Part 2. Identification of involved reaction mechanism. Fuel 167:366–374

Zeng J, Li C, Zhao L, Gao L, Du X, Zhang J, Tang L, Zeng G (2017) Removal of elemental mercury from simulated flue gas over peanut shells carbon loaded with iodine ions, manganese oxides, and zirconium dioxide. Energy Fuel 31:13909–13920

Zhang A, Zheng W, Song J, Liu Z, Xiang J (2014) Cobalt manganese oxides modified titania catalysts for oxidation of elemental mercury at low flue gas temperature. Chem Eng J 236:29–38

Zhang B, Xu P, Qiu Y, Yu Q, Ma J, Wu H, Luo G, Xu M, Yao H (2015) Increasing oxygen functional groups of activated carbon with non-thermal plasma to enhance mercury removal efficiency for flue gases. Chem Eng J 263:1–8

Zhang H, Chen J, Zhao K, Niu Q, Wang L (2016) Removal of vapor-phase elemental mercury from simulated syngas using semi-coke modified by Mn/Ce doping. J Fuel Chem Technol 44(4):394–400

Zhang J, Li C, Zhao L, Wang T, Li S, Zeng G (2017a) A sol-gel Ti-Al-Ce-nanoparticle catalyst for simultaneous removal of NO and Hg^0 from simulated flue gas. Chem Eng J 313:1535–1547

Zhang Y, Zhao L, Guo R, Wang J, Cao Y, Orndorff W, Pan W (2017b) Influences of NO on elemental adsorption characteristics for HBr modified fly ash. Int J Coal Geol 170:77–83

Zhao L, Li C, Li S, Wang Y, Zhang J, Wang T, Zeng G (2016a) Simulateous removal of elemental mercury and NO in simulated flue gas over V_2O_5/ZrO_2-CeO_2 catalyst. Appl Catal B Environ 198:420–430

Zhao B, Yi H, Tang X, Li Q, Liu D, Gao F (2016b) Copper modified activated coke for mercury removal from coal-fired flue gas. Chem Eng J 286:585–593

Zhou J, Sui Z, Zhu J, Li P, Chen D, Dai Y, Yuan W (2007) Characterization of surface oxygen complexes on carbon nanofibers by TPD, XPS and FT-IR. Carbon 45:785–796

Zhou Z, Liu X, Liao Z, Shao H, Chen L, Hu Y, Xu M (2016a) Manganese doped CeO_2-ZrO_2 catalyst for elemental mercury oxidation at low temperature. Fuel Process Technol 152:285–293

Zhou Z, Liu X, Liao Z, Shao H, Hu Y, Xu Y, Xu M (2016b) A novel low temperature catalyst regenerated from deactivated SCR catalyst for Hg^0 oxidation. Chem Eng J 304:121–128

Zhou Z, Liu X, Hu Y, Liao Z, Cheng S, Xu M (2018) An efficient sorbent based on $CuCl_2$ loaded CeO_2-ZrO_2 for elemental mercury removal from chlorine-free flue gas. Fuel 216:356–363

Zhuang Y, Laumb J, Liggett R, Holmes M, Pavlish J (2007) Impacts of acid gases on mercury oxidation across SCR catalyst. Fuel Process Technol 88:929–934